journal

Behavior of Paramagnetic Iron during the Thermal Transformations of Kaolinite

Amédée Djemai,[†,‡,§] Etienne Balan,[§] Guillaume Morin,[§] Giancarlo Hernandez,[§]
Jean Claude Labbe,[¶] and Jean Pierre Muller[†,§]

Institut de Recherches pour le Développement (IRD), Centre de Recherches d'ile de France, 93143 Bondy Cedex,
France: Laboratoire de Minéralogie-Cristallographie, UMR 7590, CNRS, Universités Paris 6 and 7, IPGP,
75252 Paris Cedex 05, France; and Sciences des Procédés Céramiques et Traitements de Surface,
Université de Limoges, UMR 6638 CNRS, 87060 Limoges, France

Kaolinites with various degrees of structural order and iron content were heated and subsequently analyzed via electron paramagnetic resonance. Iron was present in two different states in the heated materials, either as dilute structural Fe^{3+} ions or in concentrated Fe^{3+} phases. During metakaolinization, the environment of dilute Fe^{3+} ions changed, following modifications of the Al^{3+} coordination, and the Fe^{3+} concentration increased. With the breakdown of metakaolinite, the diffusion of Fe^{3+} ions induced their exsolution in superparamagnetic iron-rich domains (Fe^{3+} clusters in γ-Al_2O_3 and/or Fe^{3+} oxide nanophases), which produced a decrease in the dilute Fe^{3+} concentration. The subsequent breakdown of γ-Al_2O_3 and the formation of mullite made the dilute Fe^{3+} concentration increase again, because of the incorporation of Fe^{3+} ions in the mullite structure.

I. Introduction

MANY studies have been conducted that involve the transformation of kaolinite on heating.[1–8] At ~500°C, kaolinites dehydroxylate and transform to a pseudoamorphous phase called metakaolinite. ^{29}Si and ^{27}Al magic-angle spinning nuclear magnetic resonance (MAS NMR) studies[8] have indicated that this dehydroxylation is accompanied by changes in the Al^{3+} coordination (i.e., from local disturbances of the aluminosilicate framework). Metakaolinite decomposes, at ~980°C, to mullite,[9] poorly crystalline γ-alumina (γ-Al_2O_3), and amorphous silica (SiO_2).[6,9] However, both the occurrence and identity of the intermediate phases between metakaolinite and mullite remain the subject of much research and controversy.[2,3,6,10] A drastic change in the material structure at ~1200°C leads to the formation of a mixture of mullite and cristobalite.[9–11]

However, most of the previous studies have focused on the phase transitions that occur in the major mineralogical components of the material, and few of the studies have addressed the behavior of impurities during the thermal transformation of kaolinites. Most natural kaolinites commonly contain chemical and mineralogical impurities,[12,13] which likely influence the thermal behavior of kaolinites when they are calcined.[14] In particular, changes in the chemical status of iron and titanium, which would have undesirable effects on the optical properties of heated kaolinites,[15] are poorly known. Previous spectroscopic studies reported changes in the symmetry around paramagnetic Fe^{3+} ions on heating.[16,17] Modifications in the nature and concentration of the Fe-ion species in iron oxides were also analyzed by color changes[18] and Mössbauer spectroscopy.[19] However, neither relational nor quantitative interpretations were established between the various iron forms (i.e., dilute Fe^{3+} ions and concentrated iron phases) on calcination.

The purpose of this paper is to present a detailed study of the structural changes that are experienced by Fe ions in the aluminosilicate matrix, as a function of the firing temperature. This study mainly focuses on the electron paramagnetic resonance (EPR) analysis of the iron status, as a function of the structural changes in the aluminosilicate framework, determined by X-ray diffractometry (XRD).

Because of the high sensitivity of EPR analysis, EPR allows the detection of very small amounts of various impurities that are trapped within kaolinite particles.[20–23] Moreover, EPR allows quantification[24] and location[25] of the dilute Fe^{3+} ions by making a clear distinction between isolated Fe^{3+} ions and more-concentrated domains where the Fe—Fe distances are <6 Å.

II. Experimental Procedure

(1) Characteristics of the Samples before Heating

In this investigation, two contrasted reference kaolinite samples of fine particle size (≤2 μm) were used: highly ordered (KGa-1) and poorly ordered (KGa-2) kaolinite. The KGa-1 and KGa-2 sedimentary kaolinites originate from late Cretaceous and early Tertiary Georgia deposits, respectively. Both samples have been extensively described elsewhere[26] and were selected because of their representations of natural kaolinites. The structural order in kaolinites, as measured using XRD or EPR, is related to the iron content in the sample (see Table I). Minor quantities of anatase, goethite, and quartz are present as crystalline impurities.[23,26]

(2) Calcination Experiments

For isothermal-heating experiments, samples were loosely packed in alumina crucibles (0.3 cm³) that were inserted in an electrically heated furnace, under an air atmosphere. A Pt/Pt-Rh thermocouple that was inserted in the specimen was used to determine and maintain the temperature ($\Delta T \approx \pm 2°C$). A heating rate of 5°C/min was used to reach the set temperature. Samples were heated isothermally at the following temperatures: 200°, 300°, 500°, 700°, 900°, 950°, 1000°, 1050°, 1100°, 1150°, 1200°, and 1300°C. For each temperature, 3 h of heating were required to attain equilibrium. They were cooled at a rate of 5°C/min in air, and then each sample was ground to a powder in an agate mortar. The heated samples will be referenced using the following format: $S(T)$, where S is the sample label and T is the heating temperature

Table I. Description of Kaolinites Used

Material[†]	Impurities present[‡]	Structural order	
		HI[§]	E_{140K}[¶]
KGa-1	Anatase, quartz, 0.21% Fe_2O_3, 1.39% TiO_2	1.07	6×10^{-2}
KGa-2	Anatase, goethite, 1.13% Fe_2O_3, 2.08% TiO_2	0.21	1.5×10^{-1}

[†]Source: Provenance, Warren County, USA. [‡]Impurity content includes foreign oxides and a chemical analysis of the Fe_2O_3 and TiO_2 content.[27] [§]HI denotes the Hinckley index, or XRD index. [¶]E_{140K} denotes E measured at 140 K, where $E = L/D$ (L is the linewidth at half height, calculated on the X-band,[28] and $D = B(3Z) - B(1Y)$).

(e.g., KGa-2(200) represents a KGa-2 sample that was heated at 200°C).

(3) Characterization Methods

(A) Electron Paramagnetic Resonance: EPR spectroscopy has been described in several reviews.[29] Weighted samples were filled in calibrated silica tubes (Suprasil grade, 4 mm in diameter) at a constant height. All the EPR spectra were recorded on powder samples in a magnetic field of 0–800 mT for the X-band frequency and collected using an EPR spectrometer (Model ESP 300E, Bruker Spectrospin SA, Wissembourg, France) that was operated at an X-band frequency ($v = 9.42$ GHz). Calibration of the magnetic field was performed with a DPPH standard ($g = 2.0037 \pm 0.0002$). Frequency calibration was precisely achieved using a frequency meter (Model HP 5352 B, Hewlett-Packard, Palo Alto, CA). All the experimental parameters except the gain were kept constant for the measurements, including a modulation frequency of 100 kHz, an amplitude of 0.32 mT for the field modulation, and a time constant of 40.96 ms. A microwave power of 40 mW was chosen, because of the absence of EPR signal saturation. Low-temperature ($T = 140$ K) recording allowed strong enhancement of the paramagnetic Fe^{3+} signal, with respect to the baseline that was due to superparamagnetic iron oxides. EPR spectra were also recorded at room temperature, to study the superparamagnetic signal as a function of calcination temperature.

To gain further information about the site symmetry around the Fe^{3+} ion, Q-band EPR spectra ($v = 34$ GHz) were also recorded. These spectra were obtained in magnetic fields in the range of 0–1600 mT at $T = 140$ K for the KGa-2, KGa-2(900), and KGa-2(1300) samples.

(B) X-ray Diffractometry: Powder XRD patterns were recorded with an X-ray diffractometer (Model D500, Siemens, Karlsruhe, Germany), using CuKα radiation and a graphite monochromator. The goniometer was configured to scan over a range of 10°–70°2θ at a rate of 0.04°2θ every 20 s.

(C) Thermal Analysis: A thermoanalyzer (Type STA 409 C, Netzsch, Gerätebau Gmbh, Selb/Bavaria, Germany) was used to obtain differential thermal analysis (DTA) data in air up to 1280°C. The scan rate was 10°C/min.

III. Results

(1) Phase Transformations

(A) Aluminosilicates: The phase transformations of the aluminosilicate were similar for both starting samples KGa-1 and KGa-2. XRD patterns of unfired and heated (900°, 1000°, 1200°, and 1300°C) KGa-2 samples at various temperatures are reported in Fig. 1. Between 500°C and 700°C, the intensity of the kaolinite (001) reflection decreases and the peaks in the 18°–26°2θ range coalesce to produce a single, almost-featureless band, typical of a disordered phase, which is the major component that was observed for the KGa-2(900), KGa-2(1000), and KGa-2(1100) samples. This disordered phase persists up to 1200°C. The dehydroxylation of kaolinite, and its transformation to metakaolinite,[7] was observed on DTA curves as an endothermic peak at 545°C. Up to ~950°C, the pattern exhibits no significant change. In the XRD patterns for the KGa-2(1000) and KGa-2(1100) samples, (440), (400), and (311) reflections of γ-Al_2O_3 can be observed at 66°.50, 45°.70 and 37°.60 2θ, together with faint reflections at 16°.40 and 26°2θ; these reflections are due to the presence of mullite. At 980°C, breakdown of the metakaolinite is evidenced by an exothermic peak on the DTA curves. In the XRD pattern for the KGa-2(1200) sample, strong mullite reflections are observed and broad γ-Al_2O_3 reflections disappear. Finally, cristobalite (101) and (200) reflections can be observed in the KGa-2(1300) XRD pattern, at 21°.98 and 36°2θ, and the amorphous hump is strongly reduced. The observed transformations were consistent with earlier observations.[7–11]

(B) Foreign Oxides: In addition to kaolinite reflections, two weak peaks are observed in Fig. 1, at 25°.26 and 48°.10 2θ, and correspond to the (101) and (200) reflections of anatase. They are present as obvious resolved peaks up to 1200°C. From 900°C up to higher temperatures, a weak peak is observed at 27°.40 2θ; this peak is attributed to the (110) reflection of rutile and probably
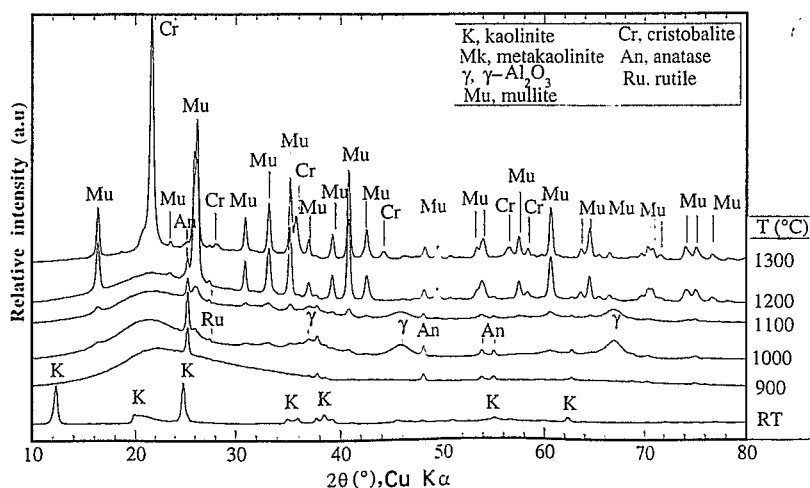

Fig. 1. XRD patterns of the original and heated kaolinite KGa-2 sample.

Table II. Phase Transformations of Kaolinites upon Calcination

Detected phases[+]	Heating temperature (°C)												
	RT[‡]	200	300	500	700	900	950	1000	1050	1100	1150	1200	1300
Aluminosilicates													
Kaolinite	X	X	X	X									
Metakaolinite				X	X	X	X						
Amorphous roll				X	X	X	X	X	X	X	X	X	
γ-Al₂O₃							X	X	X	X	X	X	
Mullite							X	X	X	X	X	X	X
Cristobalite													X
Titanium oxides													
Anatase	X	X	X	X	X	X	X	X	X	X	X	X	X
Rutile							X	X	X	X	X	X	X

ᵗFrom XRD data. ‡RT denotes room temperature.

results from the partial transformation of anatase. No iron oxide or oxyhydroxide phases were detected via XRD. However, by analogy to earlier investigations,[30,31] it is inferred that if ferric oxides/oxyhydroxides particles are present in the KGa-2 sample, their dimensions are too small to coherently scatter X-rays,[16] their concentration is below the detection limit, or both. A summary of XRD data for phase transformations in kaolinites is presented in Table II.

(2) Evolution of Structural Iron

(A) Description of X-band Electron Paramagnetic Resonance Spectra: X-band EPR spectra of the original and heated samples are presented in Figs. 2 and 3. Up to 300°C, the X-band EPR spectra show most of the resonances that have been described for natural kaolinites.[20,25,32] A complex EPR signal due to isolated Fe^{3+} ions is observed at low magnetic field ($g_{eff} = 4.27$; $B = 160$ mT). According to earlier investigations,[25,33] this signal results from the isomorphous replacement of paramagnetic Fe^{3+} ions for

Al^{3+} ions at the octahedral Al sites of the kaolinite structure, and its shape is directly related to the proportion of stacking faults within the kaolinite structure. The resonances observed at high magnetic field ($g_{eff} = 2$; $B = 330$ mT) represent an overlay of (i) a broad resonance due to superparamagnetic Fe-concentrated phases and (ii) a sharp, strong signal due to positive holes that are trapped on O atoms (these latter features have been demonstrated to be radiation-induced defects (RIDs)).[34]

The EPR spectra of all the heated products within the thermal stability field of metakaolinite (500°–900°C) show resonances at low and high magnetic fields, which corresponds to isolated Fe^{3+} ions and superparamagnetic Fe^{3+}-concentrated phases, respectively. The low-field signal is reduced to an almost-isotropic signal, which is evidence that significant changes in the site symmetry around isolated Fe^{3+} ions occur during the transformation from kaolinite to metakaolinite. At the same time, the high-field signal that is due to RIDs is strongly reduced.
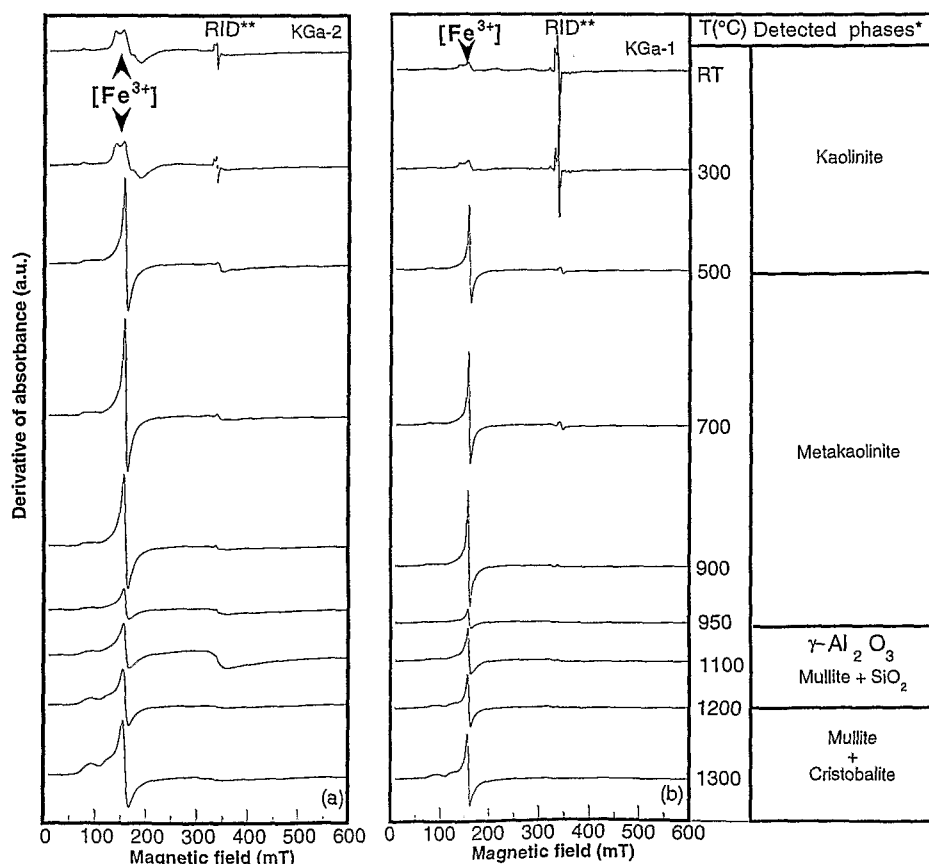

Fig. 2. EPR spectra of original and heated kaolinites ((a) KGa-2 and (b) KGa-1). Spectra obtained at 140 K. (A single asterisk (*) indicates XRD data, whereas a double asterisk (**) denotes radiation-induced defects (RIDs).)
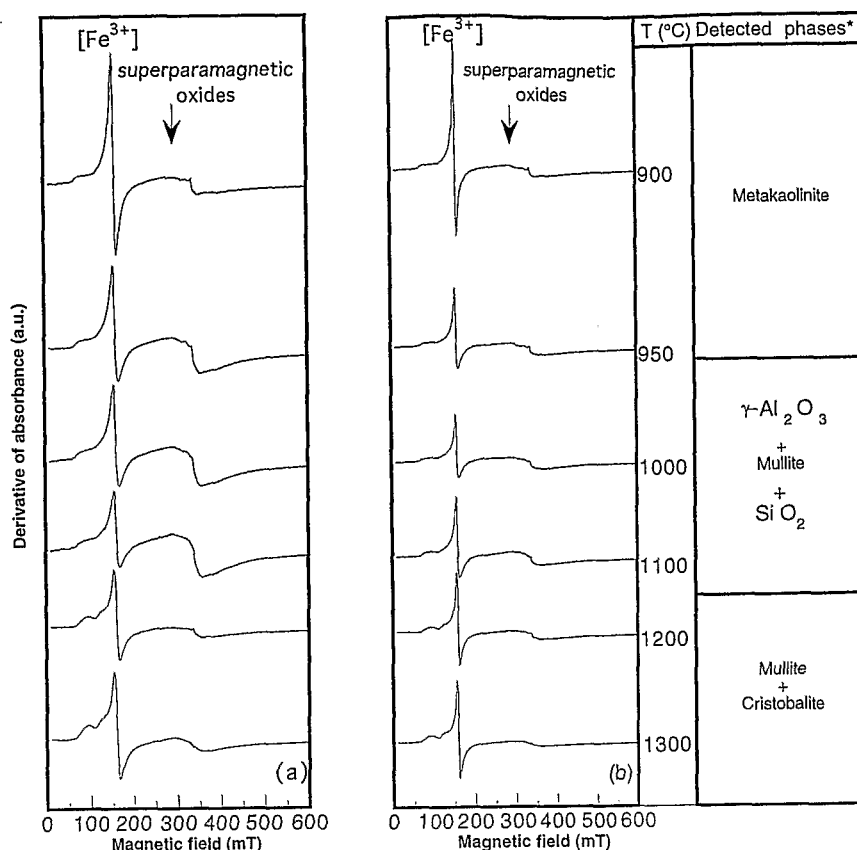
Fig. 3. EPR spectra of heated kaolinites ((a) KGa-2 and (b) KGa-1). Spectra obtained at room temperature.

At 950° and 1100°C, a broad superparamagnetic signal is observed at $g_{eff} \approx 2$ on the spectra that were recorded at low temperature (see Fig. 2). Simultaneously, the intensity of the low-field signal is strongly reduced in the spectra of both samples. Spectra that have been recorded at room temperature (see Fig. 3) exhibit a strong enhancement of this broad signal, which confirms its superparamagnetic nature.

At temperatures of >1100°C for both kaolinite samples, the low-field signal again undergoes a drastic change in shape and its intensity increases. Resonances that are observed at high magnetic field and are due to superparamagnetic iron oxides weaken but do not cancel.

(B) Characterization of Fe^{3+} Centers: The observed variation in the shape of the low-field signal between samples heated at various temperatures results from changes in the symmetry of the Fe^{3+}-coordination polyhedra. In a first approximation, the EPR spectra can be modeled in the spin Hamiltonian formalism, using the second-order fine-structure parameters B_2^0 and B_2^2.[35] A previously developed least-squares fitting method[25] allows the EPR spectra of paramagnetic ions in a disordered matrix, where the distributions of fine-structure parameters must be considered, to be modeled. Following this approach. the X- and Q-band spectra of the KGa-2, KGa-2(900), and KGa-2(1300) samples were analyzed to extract the corresponding distribution of fine-structure parameters that reflect the local symmetry around the Fe^{3+} ions. In Fig. 4, the fitted X-band EPR spectra can be compared with the experimental spectra. To obtain a satisfactory fit for both the X- and Q-bands, and to consider the superparamagnetic signal at $g_{eff} = 2$, a baseline was subtracted from the spectra. At low magnetic field ($g_{eff} \approx 4.3$), the nonzero baseline value probably results from Fe^{3+}-concentrated domains, which presents an important dipolar broadening. The corresponding distribution of fine-structure parameters for the two heated samples considered here are presented in Fig. 5.

For the unfired KGa-2 sample. the values of the fine-structure parameters primarily are concentrated in a narrow area: 0.10 cm^{-1}

$\leq B_2^0 \leq 0.13 \text{ cm}^{-1}$, and $0.06 \text{ cm}^{-1} \leq B_2^2 \leq 0.11 \text{ cm}^{-1}$. These values correspond to the parameters determined for the Fe^{3+} sites in kaolinite.[25]

For the KGa-2(900) sample, which is composed primarily of metakaolinite, the variation observed in the X-band EPR spectra corresponds to an increase in site rhombicity (i.e., B_2^2 becomes almost equal to B_2^0, and the value of B_2^0 is 0.05–0.15 cm^{-1}). However, the values of the fine-structure parameters remain concentrated primarily in a single region of the distribution map.

In contrast. the distribution map of the KGa-2(1300) sample. which is composed primarily of mullite and cristobalite, exhibits several well-defined modes that correspond to various sites that are structurally distinct. The fine-structure parameters of each mode are reported in Table III. According to the low level of Fe^{3+} incorporation[36] in cristobalite (see Fig. 6) and the similarity of the X-band spectrum of the KGa-2(1300) sample with that of Fe^{3+} centers in mullite reported by earlier investigations,[37] it can be inferred that the identified sites correspond to various sites in the mullite structure. However, direct correlation of a set of fine-structure parameters (as determined from powder EPR spectra) to a crystallographical site is difficult. Thus, a comparison of the parameters obtained on mullite to parameters that have been reported for a well-crystallized mineral of similar structure (such as sillimanite[38]) may be useful (see Table IV). EPR study on the Fe^{3+} centers in sillimanite[38] indicated two distinct sites: the low-B_2^0-value center is assigned to Fe^{3+} ions in a tetrahedral site. whereas the high-B_2^0-value center is assigned to the octahedral site (see Fig. 5). As a consequence, low-B_2^0-value centers in mullite ($0.05 \text{ cm}^{-1} < B_2^0 < 0.25 \text{ cm}^{-1}$) may be related to the tetrahedral sites T and T*[39,40] whereas high-B_2^0-value centers ($0.25 \text{ cm}^{-1} < B_2^0 < 0.4 \text{ cm}^{-1}$) may be related to octahedral sites. Note that this attribute prevents the determination of the Fe^{3+} coordination in metakaolinite from EPR data, because the fine-structure parameters of the octahedral Fe^{3+} sites in kaolinite and tetrahedral Fe^{3+} sites in mullite seem to be similar.
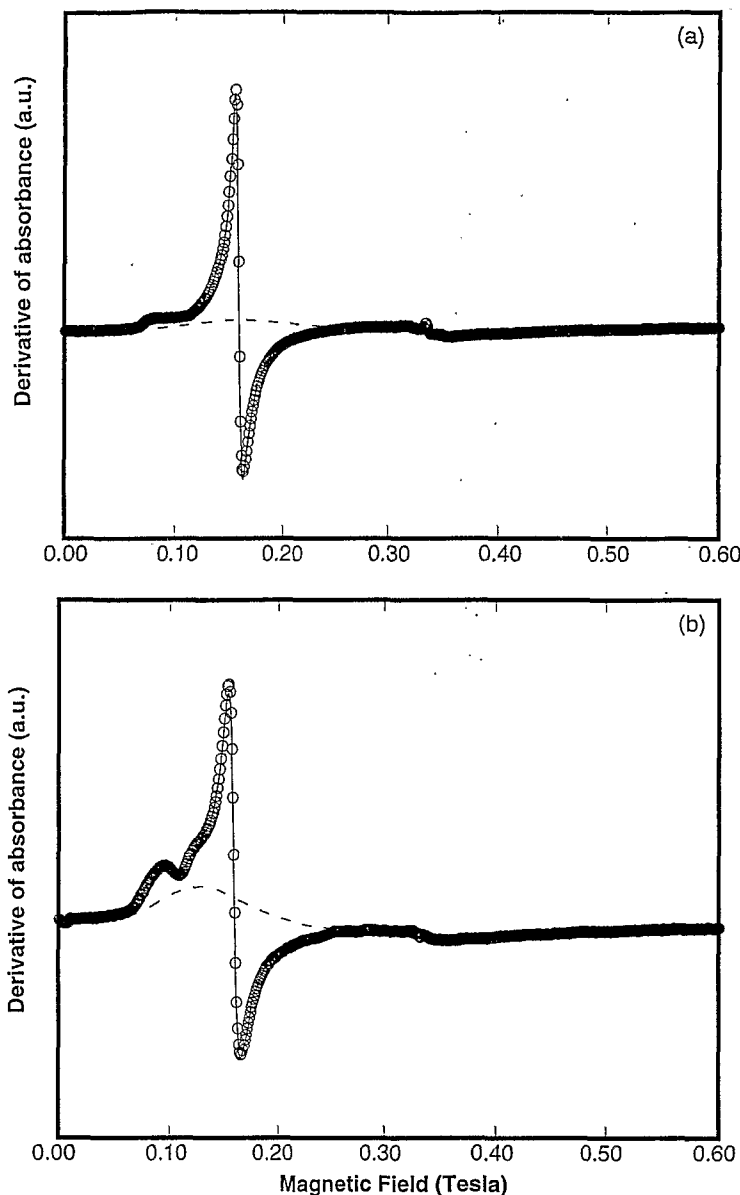
Fig. 4. Experimental and calculated X-band EPR spectra for heated kaolinite KGa-2 samples (heated at (a) 900° and (b) 1300°C). Spectra taken at 140 K. Legend is as follows: (O) experimental data, (—) calculated spectra. and (– – –) baseline.

(C) Intensity of the Paramagnetic Fe^{3+} Signal: Following the earlier procedures,[24] the paramagnetic Fe^{3+} content in the investigated samples can be determined, because the spectra were recorded under the same experimental conditions. For that purpose. the Fe^{3+} EPR signal, which is the derivative of absorbance, was integrated twice in the range of 70–270 mT for all samples. This integration includes the broad signal at $g_{eff} = 4$, which probably results from a dipolar broadened Fe^{3+} signal. The variations of the integrated EPR absorbance in Fig. 7 are reported as a function of the heating temperature.

To relate the integrated absorbances of the Fe^{3+} EPR signal to absolute concentrations, the theoretical absorbances were calculated for the various fine-structure parameters that were determined. For the mullite and metakaolinite sites, the absorbance was <10% higher than that for the kaolinite sites.

As observed in Fig. 7, the variations in the Fe^{3+} absorbance observed between kaolinite and other phases, as a function of the firing temperature, exceeds the variations that are expected from changes in the fine-structure parameters ($\leq$10%). Thus, the observed variation corresponds to an actual change in the concentration of diluted Fe^{3+} ions during the firing process. An increase in the concentration of paramagnetic Fe^{3+} ions is observed from the

original sample to the sample that was heated at 900°C, followed by a strong decrease; a minimum is attained at 950°C. Despite their contrasted iron content, the minimum value is similar for both samples. After a temperature of 1100°C, the concentration of paramagnetic Fe^{3+} ions again increases and exceeds its initial value.

IV. Discussion

In the starting materials, iron impurities are present in two different chemical forms, which are distinguished by specific signals in EPR and diffuse-reflectance spectra: (i) structural Fe^{3+} ions that are substituted for Al^{3+} ions within the dioctahedral layer of kaolinite, and (ii) particles of Fe^{3+} oxyhydroxide (i.e., goethite).[23] In addition, literature data[19] have reported the presence of Fe^{2+} ions.

During the calcination of both kaolinite samples, iron signatures in the EPR spectra undergo important modifications. In the following section, these modifications are discussed in regard to the aluminosilicate phase transformations, corresponding to the three thermal stability fields: (i) metakaolinite, (ii) γ-Al_2O_3 + mullite + SiO_2, and (iii) mullite + cristobalite.
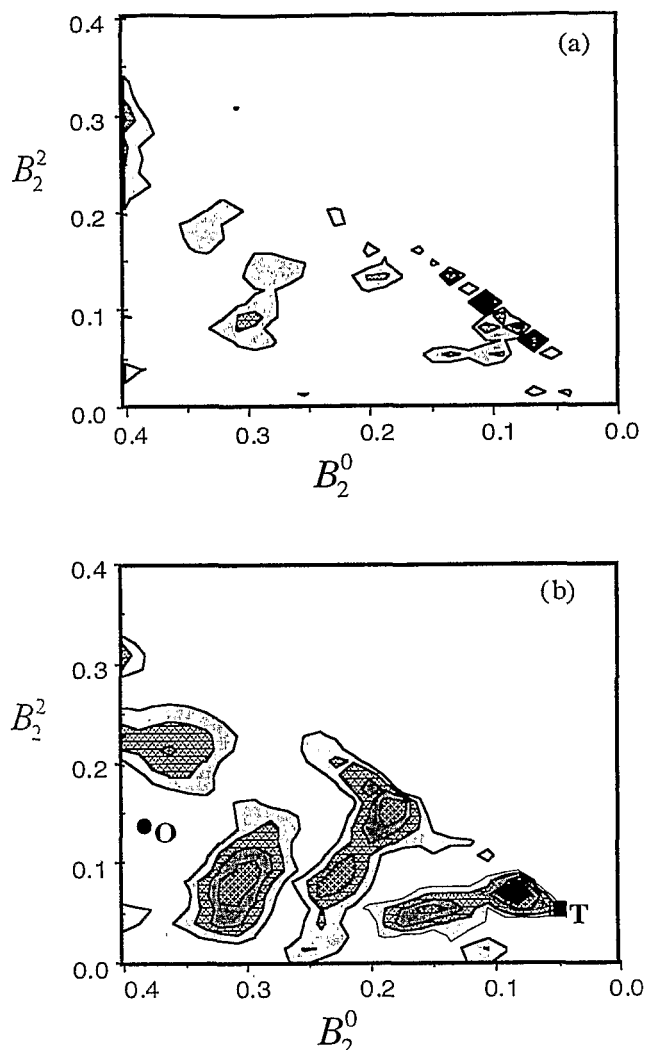
Fig. 5. Distribution map of the fine-structure parameters B_2^2 and B_2^0 (in units of cm^{-1}) for heated kaolinite KGa-2 samples (heated at (a) 900° and (b) 1300°C); the parameters of Fe^{3+} ions in octahedral (O) and tetrahedral (T) sites of sillimanite are reported in Fig. 5(b) ((●) O and (■) T).
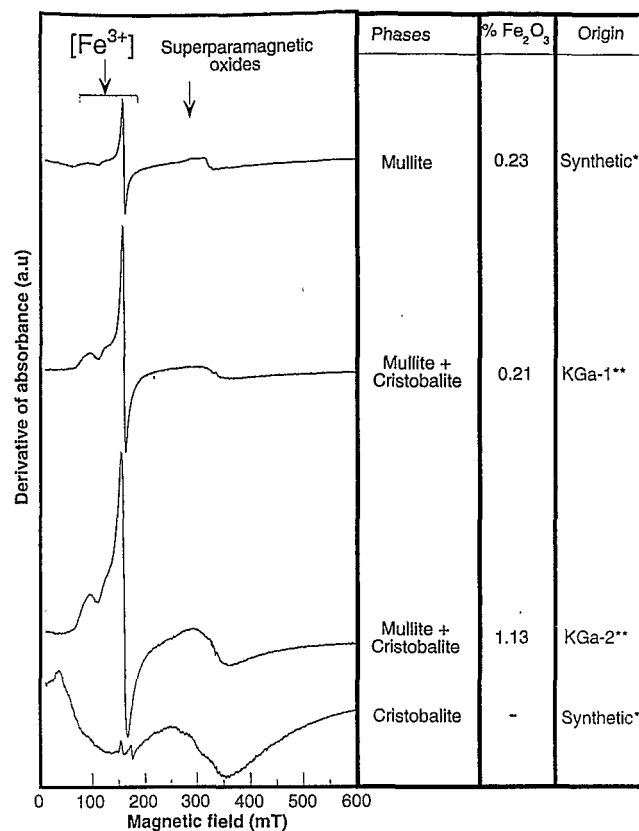

Fig. 6. Comparative EPR spectra of the reference sample and heated kaolinites ((*) data supplied by KPCL (Limoges, France) and (**) kaolinites heated up to 1300°C). Spectra obtained at room temperature.

Table III. Mean Fine-Structure Parameters of Fe^{3+} Centers in KGa-2 Kaolinite Heated at Different Temperatures

EPR site	B_2^0 (cm^{-1})	B_2^2 (cm^{-1})	λ^*
	900°C		
I	0.11	0.11	1.
	1300°C		
I	0.08	0.07	0.88
II	0.17	0.04	0.23
III	0.17	0.16	0.94
IV	0.21	0.11	0.52
V	0.29	0.08	0.27

$^*\lambda = B_2^2/B_2^0$.

Table IV. Mean Fine-Structure Parameters of Fe^{3+} Centers in Sillimanite[†]

EPR site	B_2^0 value (cm^{-1})		Structural site
	Calculated	Experiment	
I	0.11	0.06	T
V	-0.22	0.37	O

[†]Sillimanite data taken from Angel *et al.*[40]

(1) Transformation from Kaolinite to Metakaolinite

For both poorly and highly ordered kaolinite samples, the transformation from kaolinite to metakaolinite generates drastic modifications in the local environment of Fe^{3+} ions, as evidenced via EPR spectroscopy. This finding is consistent with results from Mössbauer data,[19] which presents higher quadrupole splittings after breakdown of the kaolinite.

In addition to changes in the symmetry of the local environment around the Fe^{3+} ions, variations are observed in the integrated absorbance of the paramagnetic Fe^{3+} signal. For both samples that

were heated at 700°–900°C, the Fe^{3+} concentration was >40% higher than that in the original samples. Because of the relatively low temperature of the kaolinite-to-metakaolinite transformation, iron diffusion cannot be invoked to explain such drastic changes in the diluted Fe^{3+} concentration. Mössbauer spectroscopy data that have been acquired on the KGa-1 sample[19] have shown the important contribution of Fe^{2+} ions; therefore, the increase in dilute Fe^{3+} ions might be explained by oxidation of the Fe^{2+} content of the starting kaolinites during the collapse of the kaolinite structure to form metakaolinite.

(2) Transformation from Metakaolinite to Mullite

(A) Destabilization of Metakaolinite: The strong decrease in the Fe^{3+} absorbance that has been observed for both kaolinite samples at 900°–950°C correlates with the appearance of a strong superparamagnetic signal at $g_{eff} = 2$ in the corresponding EPR spectra and the formation of γ-Al_2O_3. One must note that the residual paramagnetic Fe^{3+} concentration in metakaolinite is almost the same for both the KGa-1 and KGa-2 samples; it is not dependent on the initial iron content of the sample. Thus, one can infer that the incorporation of Fe^{3+} ions into the amorphous phase is difficult. Indeed, the drastic decrease of the amount of paramagnetic Fe^{3+} ions may be interpreted as the result of Fe^{3+} diffusion within the aluminosilicate framework and its subsequent exsolution outside of the amorphous matrix, which leads to the formation
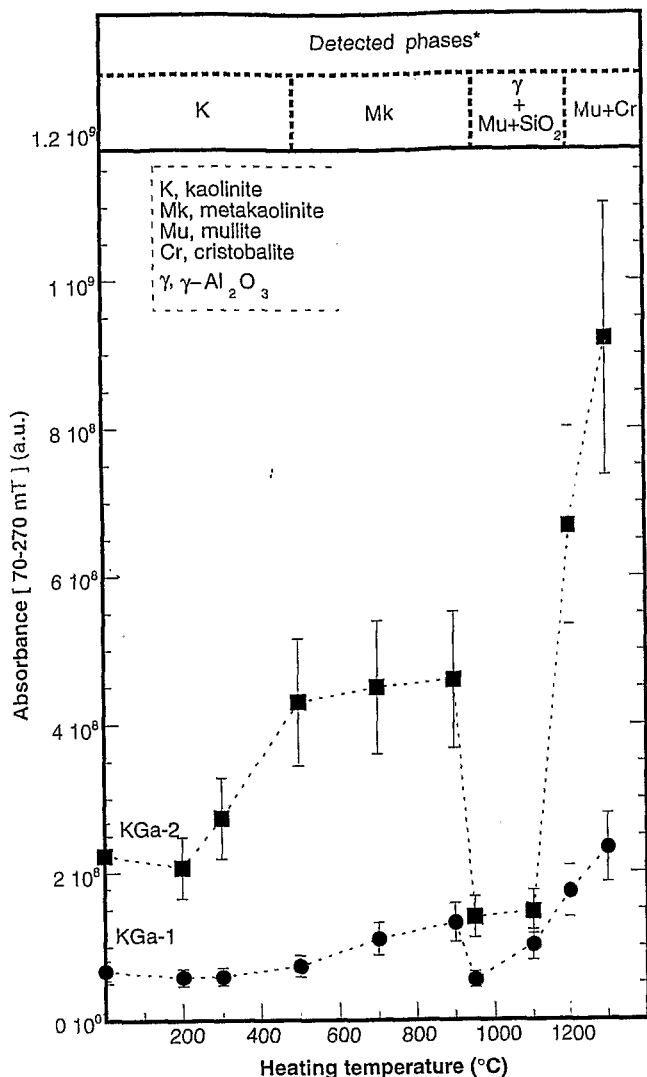
Fig. 7. Paramagnetic Fe^{3+}-ion distribution over phases in the kaolinite–mullite transformation sequence. Asterisk (*) denotes XRD data.

of superparamagnetic concentrated-iron domains. However, the nature of these iron-rich domains is unclear: they could be Fe^{3+} clusters within the γ-Al_2O_3 structure or Fe^{3+} oxide nanophases with a different structure.

(B) Mullite and Cristobalite Formation: Finally, the breakdown of the γ-Al_2O_3 and its transformation to crystalline mullite is correlated with an increase in the paramagnetic Fe^{3+} concentration, which may be interpreted as a new diffusion of Fe^{3+} ions within the aluminosilicate framework, leading to the incorporation of iron into the mullite structure. The final paramagnetic Fe^{3+} concentration exceeds the initial concentration, which indicates that the greatest portion of Fe^{3+} ions is diluted in the mullite structure. However, the possibility that residual Fe^{3+} clusters or Fe^{3+} oxide nanophases still exist in the mullite/cristobalite mixture is not excluded. Spectroscopic data on the incorporation of iron in mullite are consistent with X-ray results, in regard to the temperature dependence of Fe^{3+} solubility in mullite.[41–43]

V. Conclusion

Fe^{3+} ions undergo drastic changes in environment and concentration in heated kaolinites. These changes show important modifications that are related to phase transformations of the aluminosilicate matrix.

Iron occurs in two different states in the heated materials, either as dilute structural Fe^{3+} ions or in iron-rich domains.

Quantitative interpretation of the dilute Fe^{3+} concentration allows one to consider the process, in regard to the changes in the environment and concentration on heating, in terms of the Fe^{3+} diffusion process over phases in the kaolinite–mullite transformation sequence.

During metakaolinization, in addition to an increase in the site rhombicity of the local environment around Fe^{3+} ions, the concentration of dilute structural Fe^{3+} ions increases. The increase in the concentration of dilute Fe^{3+} ions may be related to the oxidation of Fe^{2+} ions during the collapse of the kaolinite structure to form metakaolinite.

With the breakdown of metakaolinite, the diffusion of Fe^{3+} ions induces their exsolution into superparamagnetic iron-rich domains, likely either as Fe^{3+} clusters within a γ-Al_2O_3 structure or Fe^{3+} oxide nanophases with a different structure, which leads to a decrease in the dilute Fe^{3+} concentration.

The subsequent breakdown of γ-Al_2O_3 and the simultaneous formation of mullite make the concentration of dilute Fe^{3+} ions increase again, because of the incorporation of Fe^{3+} ions in the mullite. The values of the fine-structure parameters of the Fe^{3+} ion correspond primarily to the octahedral and tetrahedral sites in the structure.

References

[1]J. F. Lambert, W. S. Millman, and J. J. Fripiat, "Revisiting Kaolinite Dehydroxylation: A ^{29}Si and ^{27}Al MAS NMR Study," *J. Am. Chem. Soc.*, 111, 3517–22 (1989).

[2](a)M. Belloto, A. Gualtiéri, G. Artioli, and S. M. Clark, "Kinetic Study of the Kaolinite–Mullite Reaction Sequence. Part I," *Phys. Chem. Miner.*, 22, 207–14 (1995). (b) M. Belloto, A. Gualtiéri, G. Artioli, and S. M. Clark, "Kinetic Study of the Kaolinite–Mullite Reaction Sequence, Part II," *Phys. Chem. Miner.*, 22, 215–22 (1995).

[3]D. Massiot, P. Dion, J. F. Alcover, and F. Bergaya, "^{27}Al and ^{29}Si MAS NMR Study of Kaolinite Thermal Decomposition by Controlled Rate Thermal Analysis," *J. Am. Ceram. Soc.*, 78 [11] 2940–44 (1995).

[4]R. L. Frost and A. M. Vassalo, "The Dehydroxylation of the Kaolinite Clay Minerals Using Infrared Emission Spectroscopy," *Clays Clay Miner.*, 44, 635–51 (1996).

[5]F. Onike, G. D. Martin, and A. C. Dunham, "Time–Temperature–Transformation Curves for Kaolinite," *Mater. Sci. Forum*, 7, 73–82 (1986).

[6]A. J. Leonard, "Structural Analysis of the Transition Phases in the Kaolinite–Mullite Thermal Sequence," *J. Am. Ceram. Soc.*, 60 [1–2] 37–43 (1977).

[7]J. Rocha and J. Klinowski, "^{29}Si and ^{27}Al MAS NMR Studies of the Thermal Transformation of Kaolinite," *Phys. Chem. Miner.*, 17, 179–86 (1990).

[8]J. Sanz, A. Madani, J. M. Serratosa, J. S. Moya, and S. Aza. "^{27}Al and ^{29}Si MAS NMR Study of the Kaolinite–Mullite Transformation," *J. Am. Ceram. Soc.*, 71 [10] C-418–C-421 (1988).

[9]X. L. Dong and W. J. Thomson, "Tetragonal to Orthorhombic Transformation during Mullite Formation," *J. Mater. Res.*, 6 [4] 819–24 (1991).

[10]A. Gualtieri and M. Bellotto, "Modelling the Structure of the Metastable Phases in the Reaction Sequence Kaolinite–Mullite by X-ray Scattering Experiments," *Phys. Chem. Miner.*, 25, 442–52 (1998).

[11]J. Rocha, J. Klinowski, and J. M. Adams, "Solid-State NMR Elucidation of the Role of Mineralizers in the Thermal Stability and Phase Transformations of Kaolinite," *J. Mater. Sci.*, 26, 3009–18 (1991).

[12]W. B. Jepson, "Structural Iron in Kaolinites and in Associated Ancillary Mineral"; pp. 467–536 in *Iron in Soils and Clay Minerals*, NATO ASI Series C, Vol. 217, Mathematics and Physical Sciences. Edited by J. W. Stucki. B. A. Goodman, and U. Schwertmann. Kluwer, Dordrecht, The Netherlands, 1987.

[13]J. P. Muller, A. Manceau, J. L. Hazemann, T. Allard, P. Ildefonse, and G. Calas, "Crystal Chemistry of Clays and Associated Oxides: Constraints for Modelling Element Transfer at the Earth's Surface," *Am. J. Sci.*, 295, 1115–55 (1995).

[14]T. Kendall, "Kaolinitic Refined Clays"; pp. 53–70 in *Industrial Clays*, 2nd Ed., 1996.

[15]P. Sennet, "Changes in the Physical Properties of Kaolin on Exposure to Elevated Temperature," *Sci. Geol. Mem.*, 89, 71–79 (1990).

[16]L. Stoch, "Iron in Kaolins—Mineralogical, Crystalo-Chemical and Technological Aspects," *Interceram.*, 6, 21–25 (1987).

[17]T. Watanabe, H. Shimizu, K. Nagasawa, A. Masuda, and H. Saito, "^{29}Si and ^{27}Al MAS/NMR Study of the Thermal Transformations of Kaolinite," *Clay Miner.*, 22, 37–48 (1987).

[18]C. S. Hogg and F. R. Noble, "A Kubelka-Munk Analysis of the Influence of Iron and Titanium Oxides on the Optical Properties of Hard Porcelain," *Sci. Ceram.*, 10, 703–10 (1979).

[19]E. Murad and U. Wagner, "Mossbauer Spectra of Kaolinite, Halloysite and the Firing Products of Kaolinite: New Results and a Reappraisal of Published Work," *Neues Jahrb. Mineral. Abh.*, 162 [3] 281–309 (1991).

[20]J. P. Muller and G. Calas, "Genetic Significance of Paramagnetic Centers in Kaolinites"; pp. 261–89 in *Kaolin Genesis and Utilization*. Edited by H. H. Murray, W. M. Bundy, and C. C. Harvey. The Clay Minerals Society of America, Boulder, CO, 1993.

[21]J. M. Gaite, P. Ermakoff, and J. P. Muller, "Characterization and Origin of Two Fe^{3+} EPR Spectra in Kaolinite," *Phys. Chem. Miner.*, 20, 242–47 (1993).

[22]T. Delineau, T. Allard, J. P. Muller, O. Barres, J. Yvon, and J. M. Cases, "FTIR vs. EPR Studies of Substituted Fe^{3+} in Kaolinite," *Clays Clay Miner.*, **42**, 308–20 (1994).

[23]N. Malengreau, J. P. Muller, and G. Calas, "Fe-Speciation in Kaolins: A Diffuse Reflectance Study," *Clays Clay Miner.*, **42**, 137–47 (1994).

[24]E. Balan, T. Allard, B. Boizot, G. Morin, and J.-P. Muller, "Quantitative Measurement of Paramagnetic Fe^{3+} in Kaolinite," *Clays Clay Miner.*, **48** [4] 439–45 (2000).

[25]E. Balan, T. Allard, B. Boizot, G. Morin, and J.-P. Muller, "Structural Fe^{3+} in Natural Kaolinites: New Insights from EPR Spectra Fitting at X and Q-Band Frequencies," *Clays Clay Miner.*, **47** [5] 605–16 (1999).

[26]H. H. Murray, "Kaolin Minerals, Their Genesis and Occurrences"; pp. 67–89 in *Hydrous Phyllosilicates*, Reviews in Mineralogy, Vol. 19. Edited by S. W. Bailey. Mineralogical Society of America, Washington, DC, 1988.

[27]H. V. Olphen and J. J. Fripiat, *Data Handbook for Clay Materials and Other Non-Metallic Minerals*. Pergamon Press, London, U.K., 1979.

[28]J. M. Gaite, P. Ermakoff, T. Allard, and J. P. Muller, "Paramagnetic Fe^{3+}: A Sensitive Probe for Disorder in Kaolinite," *Clays Clay Miner.*, **45** [4] 496–505 (1997).

[29]G. Calas, "Electron Paramagnetic Resonance"; pp. 513–63 in *Spectroscopic Methods in Mineralogy and Geology*, Reviews in Mineralogy, Vol. 18. Edited by F. C. Hawthorne. Mineralogical Society of America, Washington, DC, 1988.

[30]W. Kundig, H. Bommel, R. H. Linquist, G. Constabaris, and R. H. Lindquist, "Some Properties of Supported Small α-Fe_2O_3 Particles Determined with the Mössbauer Effect," *Phys. Rev.*, **142**, 327–33 (1966).

[31]R. V. Morris, D. G. Agresti, H. V. Lauer, J. A. Newcomb, T. D. Sheler, and A. V. Murali, "Evidence for Pigmentary Hematite on Mars Based on Optical, Magnetic and Mossbauer Studies of Superparamagnetic (Nanocrystalline) Hematite," *J. Geophys. Res.*, **94** [B3] 2760–78 (1989).

[32]R. E. Meads and P. J. Malden, "Electron Spin Resonance in Natural Kaolinites Containing Fe^{3+} and Other Transition Metal Ions," *Clay Miner.*, **10**, 313–45 (1975).

[33]B. R. Angel and W. E. J. Vincent, "Electron Spin Resonance Studies of Iron Oxides Associated with the Surface of Kaolins," *Clays Clay Miner.*, **26**, 263–72 (1978).

[34]T. Allard, J. P. Muller, J.-C. Dran, and M. T. Menager, "Radiation Induced Paramagnetic Defects in Natural Kaolinites: Alpha Dosimetry with Ion Beam Irradiation," *Phys. Chem. Miner.*, **21**, 85–96 (1994).

[35]A. Abragam and B. Bleaney, *Electron Paramagnetic Resonance of Transition Ions*. Clarendon Press, Oxford, U.K., 1970.

[36]H. Schneider and A. Majdic, "Iron Incorporation in Tridymite and Cristobalite," *Neues Jahrb. Mineral., Monatsh.*, **H.12**, 559–68 (1984).

[37]H. Schneider and H. Rager, "Iron Incorporation in Mullite," *Ceram. Int.*, **12**, 117–25 (1986).

[38]J. Le Marshall, D. R. Hutton, G. J. Troup, and J. R. W. Thyer, "A Paramagnetic Resonance Study of Cr^{3+} and Fe^{3+} in Sillimanite," *Phys. Status Solidi A*, A5, 769–73 (1971).

[39]R. J. Angel and C. T. Prewitt, "Crystal Structure of Mullite: A Reexamination of the Average Structure," *Am. Mineral.*, **71**, 1476–82 (1986).

[40]R. J. Angel, R. K. McMullan, and C. T. Prewitt, "Substructure and Superstructure of Mullite by Neutron Diffraction," *Am. Mineral.*, **76**, 332–42 (1991).

[41]H. Schneider, "Temperature-Dependent Iron Solubility in Mullite," *J. Am. Ceram. Soc.*, **70** [3] C-43–C-45 (1987).

[42]M. K. Murthy and F. A. Hummel, "X-Ray Study of the Solid Solution of TiO_2, Fe_2O_3, and Cr_2O_3 in Mullite ($3Al_2O_3 \cdot 2SiO_2$)," *J. Am. Ceram. Soc.*, **43** [5] 267–71 (1960).

[43]W. E. Brownell, "Subsolidus Relations between Mullite and Iron Oxide," *J. Am. Ceram. Soc.*, **41** [6] 226–30 (1958). □
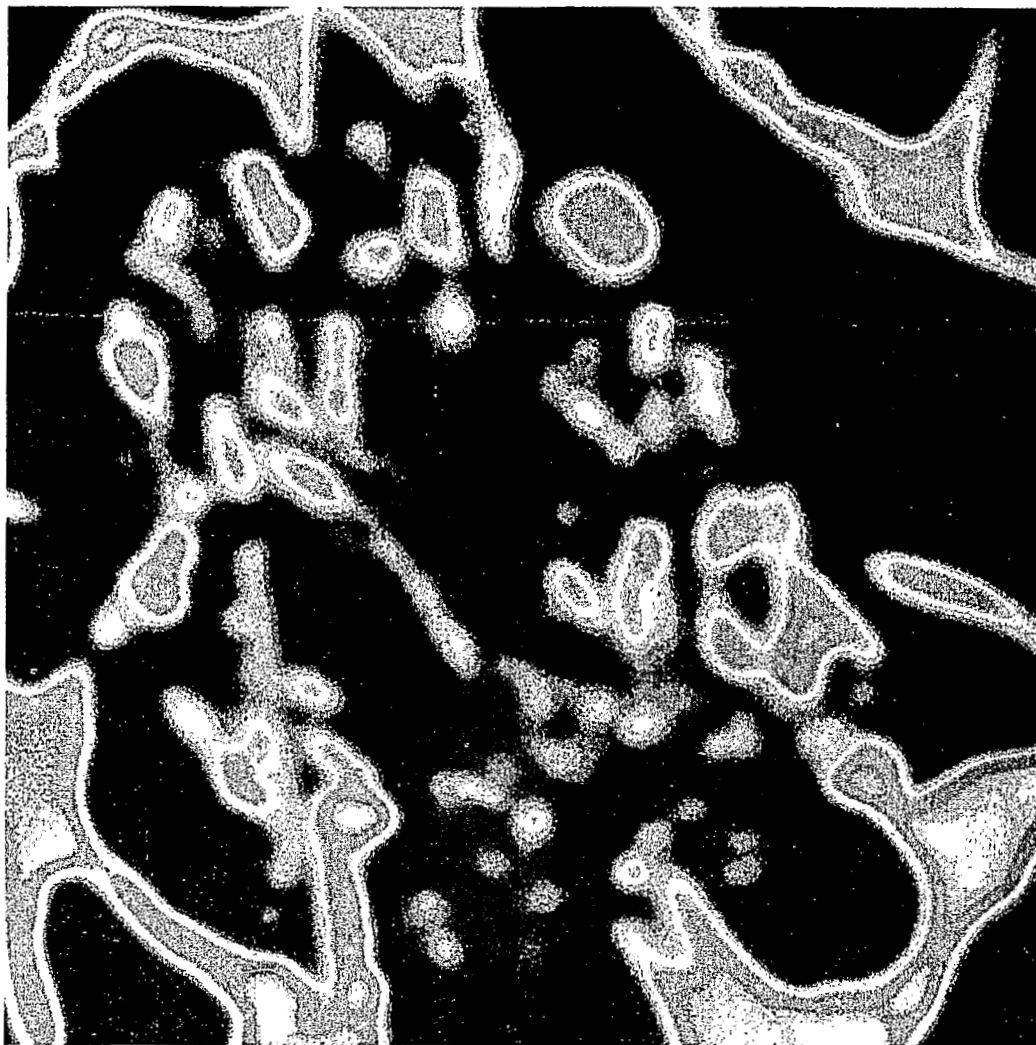
Journal

of the American Ceramic Society

Incorporating Advanced Ceramic Materials and Communications

Volume 84   Number 5   May 2001